CARBON letters

Original Articles
Carbon Letters Vol. 22, 25-35 (2017)

Thermo-electrical properties of randomly oriented carbon/carbon composite

Thakur Sudesh Kumar Raunija[1,♠] and N. Supriya[2]

[1]Carbon and Ceramics Laboratory (CCL), Materials and Mechanical Entity, Vikram Sarabhai Space Centre, Indian Space Research Organisation, Thiruvananthapuram 695022, India
[2]Analytical and Spectroscopy Division (ASD), Propellants Polymers Chemicals and Materials Entity, Vikram Sarabhai Space Centre, Indian Space Research Organisation, Thiruvananthapuram 695022, India

Article Info
Received 12 August 2016
Accepted 18 February 2017

♠Corresponding Author
E-mail: thakurskr@gmail.com
Tel: +91-471-2562979

Open Access
DOI: http://dx.doi.org/10.5714/CL.2017.22.025

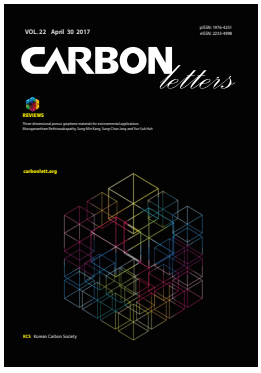

http://carbonlett.org

pISSN: 1976-4251
eISSN: 2233-4998

Abstract

The aim of the work was to investigate the thermo-electrical properties of low cost and rapidly produced randomly oriented carbon/carbon (C/C) composite. The composite body was fabricated by combining the high-pressure hot-pressing (HP) method with the low-pressure impregnation thermosetting carbonization (ITC) method. After the ITC method step selected samples were graphitized at 3000°C. Detailed characterization of the samples' physical properties and thermal properties, including thermal diffusivity, thermal conductivity, specific heat and coefficient of thermal expansion, was carried out. Additionally, direct current (DC) electrical conductivity in both the in-plane and through-plane directions was evaluated. The results indicated that after graphitization the specimens had excellent carbon purity (99.9 %) as compared to that after carbonization (98.1). The results further showed an increasing trend in thermal conductivity with temperature for the carbonized samples and a decreasing trend in thermal conductivity with temperature for graphitized samples. The influence of the thickness of the test specimen on the thermal conductivity was found to be negligible. Further, all of the specimens after graphitization displayed an enormous increase in electrical conductivity (from 190 to 565 and 595 to 1180 S/cm in the through-plane and in-plane directions, respectively).

Key words: Exfoliated carbon fibers, specific heat, thermal diffusivity, thermal conductivity, CTE

1. Introduction

The potential value of carbon/carbon (C/C) composites as a material for high temperature applications was recognized at a very early stage, and led to their practical development in the 1960s. Initially developed as materials for thermal protection during space vehicle re-entry, later the composites were used for the fabrication of thermo-structural components such as the nose cone, wing leading edges, etc. [1-3]. In the last couple of years, in addition to these specialized thermo-structural uses, their applications have been extended to non-thermo-structural components such as molecular sieves, heat sinks [4, 5], metal to glass sealing support fixtures [6, 7], international thermonuclear experimental reactor (ITER) plasma facing components [8], bipolar plates [9-12], etc. High thermal and electrical conductivities are key requirements of these non-thermo-structural components.

Carbon based materials exhibit the highest measured thermal conductivity of any known material at moderate temperatures. For practical applications, the engineering utility of carbon materials in the form of composites has been extensively studied. For example, continuous carbon fiber reinforced C/C composite has been the focus of various researchers [13-21]. Multiple approaches have been developed for making continuous C/C composite, including fabrication methods with pyrolytic graphite, using

chemical vapor infiltration (CVI), metallurgical products' hot isostatic pressure impregnation carbonization (HIPIC) and hand layup. But while the continuous carbon fiber reinforced C/C composites produced by these processes have excellent mechanical properties, each process is associated with one or more issues. C/C composite made out of CVI is costly and time consuming, whereas the HIPIC method is cost intensive. For these reasons, C/C composite applications are presently limited to high end uses such as aerospace and defense.

To expand the use of C/C composite materials to additional commercial applications, methods must be developed to produce it rapidly at low cost. To accomplish this, a slight compromise in mechanical properties is permissible. Recently, short carbon fiber composites have attracted the attention of designers and material scientists because they are easier to fabricate and also offer the possibility of achieving isotropic properties. Significant efforts have since been invested in reducing the processing time and cost of these C/C composites. For example, Klett et al. [22] demonstrated a fast fabrication route for the composites. Raunija et al. [6] also developed a rapid process for the fabrication of short carbon fiber reinforced C/C composite.

Nonetheless, detailed studies on the thermo-electrical properties of short fiber reinforced C/C composites are still not widely available in the open literature. This is not the case for continuous C/C composites, where various properties such as thermal, mechanical and electrical characteristics have been investigated in detail. Manocha and co-workers [23, 24] have studied the thermophysical properties of continuous (1-D and 2-D) C/C composite. Reports are also available on the thermal properties of continuous fiber reinforced polymer matrix composite [25] and chopped carbon fiber reinforced polymer matrix composite [26].

Our group has done extensive work on randomly oriented short fiber reinforced C/C composite at the Vikram Sarabhai Space Centre [27-33], however, the details of its thermo-electrical properties have not been reported so far. Accordingly, a detailed investigation of the thermo-electrical properties of the short fiber reinforced C/C composite system was carried out in this work.

2. Experimental

2.1. Materials used

High modulus and high conductivity pitch based P75, and high strength polyacrylonitrile based T800 carbon fibers, were used as reinforcement. After stabilization, petroleum pitch derived isroaniso matrix precursor (IMP) was used as the primary matrix precursor (PMP) for the derivation of the primary carbon matrix (PCM). IMP is a special mesophase pitch synthesized at the Carbon and Ceramics Laboratory (CCL) of Vikram Sarabhai Space Centre via a thermotropic route. In-house synthesized resole type phenol formaldehyde resin (PF106) was used as the secondary matrix precursor (SMP) for deriving the secondary carbon matrix (SCM). Distilled water produced in-house through a double distillation set-up was used as the slurry media.

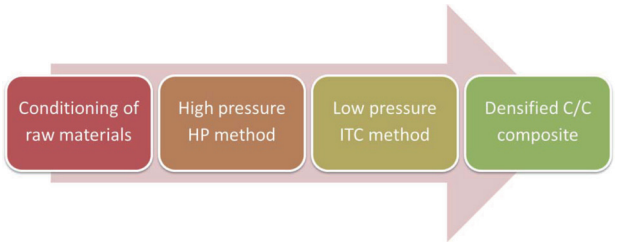

Fig. 1. Process flow diagram. HP, hot-pressing; ITC, impregnation thermosetting carbonization; C/C, carbon/carbon.

2.2. Fabrication of the C/C composite

Fig. 1 shows a block diagram of the processing stages of the C/C composite. The raw materials (carbon fibers and IMP) were first conditioned. The as-received continuous carbon fibers were chopped into discrete lengths using a custom developed fiber milling machine and method of milling [34]. The chopped fibers were then exfoliated using an in-house exfoliation set-up [6] and the exfoliated carbon fibers were used as reinforcement. The IMP was stabilized in air to get the stabilized matrix precursor [32]. It was then used as the PMP.

After conditioning of the raw materials, the C/C composite was fabricated in two steps. In the first step, a medium density C/C composite was fabricated using the primary high pressure HP method [32]. In the primary method, a slurry of exfoliated carbon fibers and the stabilized IMP was prepared by agitating them in distilled water. The well mixed slurry was then vacuum moulded to produce green cake. The green cake was dried in an air oven to get preform. The preform thus made was hot pressed at 700°C with the heating rate of 0.2°C/min for 180 min to bind the reinforcement. PCM was derived from the PMP as a result of pyrolysis, and subsequent carbonization at 1050°C for 60 min to produce a medium density C/C composite. The C/C composite thus obtained was further densified in a second step using the low-pressure impregnation thermosetting carbonization (ITC) method [29, 30]. In this step, the pores of the C/C composite were evacuated under vacuum, followed by impregnation with phenol formaldehyde resin, thermosetting, and finally carbonization of the infiltrated phenol formaldehyde. The entire cycle of pore evacuation-resin infiltration-thermosetting-carbonization of the low-pressure ITC method was repeated three times. The first cycle is called DC1, the second DC2 and the third DC3.

After completing the two step processing, selected samples were graphitized at 3000°C in a custom developed graphitization furnace at 50°C/min for a duration of 10 min.

2.3. Characterization of the C/C composite

2.3.1. Physical properties

Investigation of the as-produced composite's microstructure was carried out with an Olympus optical metallurgical microscope. After resin mounting small sized specimens, conventional metallographic techniques were used for polishing the speci-

mens with different grades of emery papers. The final polishing was carried out with 1μm diamond paste. The microstructure was evaluated by the ITC method in both through-plane and in-plane directions.

The bulk density of compact samples after the hot-pressing and carbonization stages of the primary fabrication method, after each complete cycle of the secondary method, and after the graphitization step was calculated using the mass-volume formula given below:

$$\rho_h = \frac{m}{v} \quad (1)$$

where,
ρ_h = bulk density of the compact (g/cm^3),
m = mass of the compact (g),
v = volume of the compact (cm^3).

Carbon content analysis of the raw materials and the composite samples was evaluated following the HP method step, the ITC method step, and the graphitization step, by CHNS analyzer (2400 Series II; PerkinElmer, USA). For accurate measurement of the carbon content, a small quantity (0.1 g) of the sample was burnt with oxygen in the furnace at 1000°C. In the presence of oxygen, the carbon content present in the test sample is converted into carbon oxides. The analysis of the combustion product was carried out by thermal conductivity detector to obtain the carbon content.

The wt% of each constituent (carbon fibers and the carbon matrix derived from PMP and SMP) in the composite was determined after the high-pressure HP method step and the low-pressure ITC method step. Further, the deposition profile of the SCM was determined following the densification cycles of the ITC method step. The determination of graphitizable carbon (GC) and non-graphitizable carbon (NGC) was also done after the ITC method step. To accurately measure the wt% of each constituent in the composite, the weight loss of both types of carbon fibers up to carbonization stage was estimated by TGA studies, and was appropriately deducted to determine the wt% of the PCM and SCM in the C/C compact. The applicable equations used for the wt% computation are given below:

$$w_p = w_{cf} + w_{pmp} \quad (2)$$

$$w_{HP} = w_{cf} + w_{pcm} \quad (3)$$

$$w_{ITC} = w_{cf} + w_{pcm} + w_{scm} \quad (4)$$

where
w_p = weight of the preform (g),
w_{pmp} = weight of the primary matrix precursor in preform (g),
w_{cf} = weight of the carbon fiber (g),
w_{HP} = weight of the compact after the HP method step (g),
w_{ITC} = weight of the compact after the ITC method step (g),
w_{pcm} = weight of the PCM in the compact (g),
w_{scm} = weight of the SCM in the compact (g).

An X-ray diffraction (XRD) study was conducted using an X-ray diffractometer (Panalytical Xpert Pro MPD, the Netherlands). The data was collected at a scan rate of 3°/min using CuKα radiation at 40 kV and 30 mA. XRD was conducted for the as-received raw materials, the individually processed raw materials at high-pressure HP method conditions, the C/C compacts after the high-pressure HP method step, low-pressure ITC method step and graphitization step.

The XRD of the raw materials and the C/C composite was conducted after different processing stages to determine the behavior of the degree of graphitization with each of the processing stages. The degree of graphitization can be calculated using empirical equations. There are four methods which co-relate the degree of graphitization to the XRD diffraction values obtained experimentally. They include the Franklin method (p factor), the Bacon method (p factor), the Maire and Mering method (g factor) and the Warren Method (P_1) [35]. The Maire and Mering method is the most common and easy way to calculate the degree of graphitization. Therefore, it was used to calculate the degree of graphitization as follows:

$$\%g = \frac{(0.344 - d_{(002)})}{(0.344 - 0.3354)} \quad (5)$$

Where
%g = degree of graphitization,
0.344 = interlayer spacing for non - graphitized carbon,
0.3354 = interlayer spacing for ideal graphite crystallite,
$d_{(002)}$ = interlayer spacing dervied from XRD.

Interlayer spacing ($d_{(002)}$) can be calculated by the Bragg equation, and using this value in the model given by Maire and Mering, the value of degree of graphitization can be computed [36]. The non-graphitized carbon is called turbostratic graphite [37].

2.3.2. Thermal properties

Thermal properties including diffusivity, conductivity and specific heat were measured in both the in-plane and through-plane directions after the primary method step, the secondary method step and graphitization step using a Flashline-3000 thermal property analyzer (FL-3000; Anter Corp., USA) as per American Society for Testing and Materials (ASTM) E1461-13. A thin disc of the sample of Ø12.7 mm was placed in the sample holder. After heat insulation, the front side of the sample was subjected to a very short burst of energy from a high speed xenon discharge pulse source, producing a one dimensional heat flow at the rear side of the sample. The temperature rise on the rear side was measured using an infrared detector. The entire test was performed under argon atmosphere. Thermal diffusivity (α) and conductivity (k) were obtained directly from the instrument by considering the density. Specific heat was then calculated indirectly using the following equation:

$$C_p = \frac{\lambda}{\rho.\alpha} \quad (6)$$

where,
α = thermal diffusivity (cm^2/s),
λ = thermal conductivity (w/mk),
ρ = density (g/cm^3),
C_p = specific heat.

The coefficient of thermal expansion (CTE) of the samples was measured for both the in-plane and through-plane directions from RT to 1000°C using a TA Instruments Q-400 thermomechanical analyzer as per ASTM E831-12. A composite sample of 5 mm×5 mm×5 mm in contact with the TMA probe was heated from RT to 1000°C at 10°C/min under nitrogen atmosphere at a purge rate of 100 mL/min to measure the CTE in a Q-400 thermomechanical analyzer. An average of 3 samples was reported.

2.4. Electrical properties

The direct current (DC) electrical conductivity of the samples in both the in-plane and through-plane directions after the low-pressure ITC method step and the graphitization step was measured by the 4 point method as per ASTM D257-07. A Fluke 5520 multifunction calibrator and HP 3458A digital multimeter were used to measure conductivity at a temperature of 23±2°C and relative humidity of 60±5%. An average of 5 samples (rectangular cross-section) was reported. The conductivity was computed as follows:

$$E = \frac{t}{a.R} \quad (7)$$

where

E = electrical conductivity (S/cm),

a = the effective area of the measuring electrode (cm^2),

R = measured volume resistance (Ω),

t = average thickness of the specimen (cm).

3. Results and Discussion

3.1. Physical properties

3.1.1. Microstructure

Fig. 2 shows the optical microscopy micrographs of the composite samples taken after the low-pressure ITC method step. The micrograph of the through-plane, shown in Fig. 2a, clearly shows the alignment of most of the carbon fibers in the x-y plane, whereas the micrograph of the in-plane, shown in Fig. 2b, shows only ends of carbon fibers, which also validates the x-y plane alignment of the carbon fibers. Further, it can be seen that the distribution of carbon fibers, both PCM and SCM, is very uniform throughout the surface. The micrographs indicate the samples are entirely free of pores, cracks and de-laminations. Almost all the carbon fiber filaments are interconnected, which is highly desirable for good conduction as per percolation theory. The impact of this is discussed in later sections of the paper.

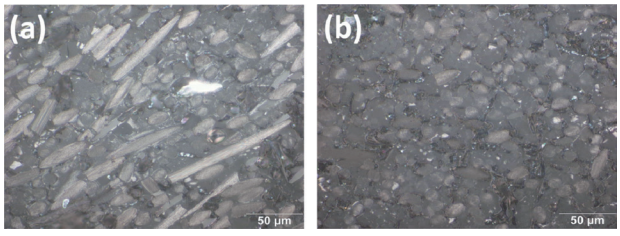

Fig. 2. Optical microscopy images after the ITC method step; (a) through-plane, (b) in-plane.

3.1.2. Density

Density as high as 1.64 g/cm^3 was measured just after the HP method step after a processing time of less than 64 h. From a processing point of view, that obtained density is significantly high as compared to conventional processes such as HIPIC, liquid polymer infiltration (LPI) and CVI. The obtained C/C composite was further densified with a densifier step. Significant improvement in the density (from 1.64 to 1.75 g/cm^3, by 6.7%) was achieved with the low-pressure ITC method at an additional processing time of 73 h.

The step by step change in density can be described as follows. An appreciable enhancement in density (from 1.64 to 1.70 g/cm^3 by 3.7%) was recorded after the first ITC cycle. However, the percentage increase in density during the second ITC cycle (from 1.70 to 1.73 g/cm^3 by 1.8%) and the third ITC cycle (from 1.73 to 1.75 g/cm^3 by 1.2%) was comparatively less than that of the first cycle (3.7%). The density increase in the compact after the third ITC cycle was comparatively very low. That shows that further usage of ITC cycles in this particular method of C/C fabrication is not significant. The total fabrication time of the C/C composite up to the third ITC cycle was only 137 h.

It should be noted that the conventional process takes around 3 months (180 days) to achieve a similar density of C/C composite. The appropriate use of the high-pressure HP method and low-pressure ITC method yielded C/C composite in a much shorter time. Selected samples were graphitized to determine its impact on the composite's properties. The density was found to increase with graphitization due to shrinkage.

3.1.3. Carbon content

The carbon content of the compacts was determined after the HP method, ITC method and graphitization steps. This was mainly done to determine the purity of the C/C composite in terms of carbon content, so that its application could be decided accordingly.

Table 1 shows the carbon content of all the raw materials and the variation in the carbon content of the C/C composite with each processing step. From Table 1, it can be clearly seen that the carbon content after the HP method step has increased significantly compared with that of its constituents. The increase in the carbon content of the C/C composite after the HP method step is mainly produced by the pyrolysis and carbonization of the PMP [38]. After further densification cycles, it remains almost the same. After graphitization, the value of carbon content reaches almost 100% (99.9% actual). This demonstrates the ultra-high purity of the C/C composite in terms of carbon content. This purity is due to the liberation of even tightly bound hetro-atoms at the graphitization temperature. Ultra-high purity is most important for high temperature applications of the C/C composite because the presence of even a minute quantity of non-carbonaceous matters may result in deviation from expected properties due to degassing of these non-carbonaceous matters at the application temperature.

Table 1. Carbon content of raw materials and the carbon/carbon composite at different processing stages

Constituent	Raw materials				Processing stages		
	P75	T800	PM	SM	HP method	ITC method	Graphitization
C	99.6	96	87.5	75.3	98.6	98.5	99.9

HP, hot-pressing; ITC, impregnation thermosetting carbonization.

3.1.4. Composition analysis

Composition analysis (the wt% contribution of each type of carbon) of the compacts was performed after the HP method and ITC method steps. Fig. 3 shows the wt% contribution of the T800, P75, PCM and SCM in the compact after the HP method and ITC method steps. The pattern of SCM deposition with the ITC cycles was also checked. The main objective of this analysis was to gain some idea of the % contribution of GC and NGC in the C/C composite. The PCM derived from the PMP differs in properties from SCM derived from SMP. Hence, the % contribution of PCM and SCM plays an important role in estimating the final properties of the composite.

The PCM was developed in a single step during the primary HP method. The SCM was developed gradually with densification cycles during the secondary ITC method step. In DC1, the wt% of SCM developed was 70% of the total; this increased to 94% of the total in DC2, and to 100% of the total in DC3. The sequential development of SCM with densification cycles is given in Fig. 3. This calculation also helps in deciding the effective number of densification cycles. As is clear from the DC2 and DC3 results, the development of SCM in those cycles is marginal. Hence, further impregnation will not result in additional densification of the C/C composite. This is because either the pores are filled or the pore diameter is too small to allow the further infiltration of resin.

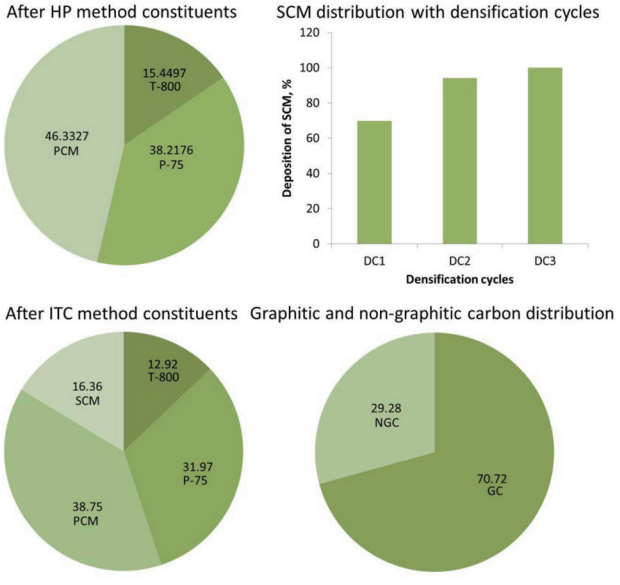

Fig. 3. Composition analysis. HP, high pressure; SCM, secondary carbon matrix; DC, direct current; ITC, impregnation thermosetting carbonization; PCM, primary carbon matrix, GC, graphitizable carbon; NGC, non-GC.

3.1.5. X-ray diffraction

Fig. 4 shows the XRD patterns of the as-received raw materials, the ball milled raw materials in the same proportion used to prepare the C/C composite, and the individually processed raw materials at the C/C composite processing conditions. From peak broadening, it can be seen that the pattern of carbon fibers remains almost the same after processing at the C/C composite preparation conditions. However, although the broad peaks correspond to amorphous carbon, minute changes in the pattern of the PMP can be seen after processing. This can be attributed to the fact that the carbonization of PMP took place during processing [36]. Further, the XRD patterns of the as-received raw materials, ball milled raw materials and C/C composite at different stages of the high-pressure HP method are shown in Fig. 5. It can be clearly seen that the peaks of the C/C composite mainly correspond to those of P75 carbon fiber.

A detailed analysis of the influence of ingredients on the

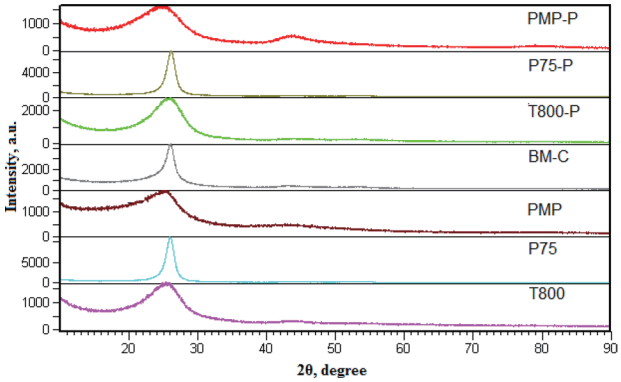

Fig. 4. X-ray diffraction patterns of raw materials.

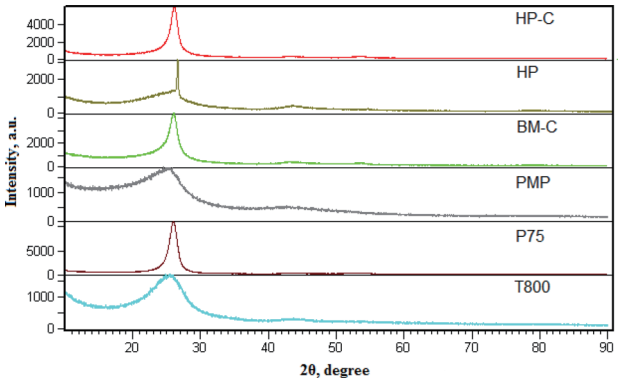

Fig. 5. X-ray diffraction patterns of raw materials along with processed carbon/carbon composite.

graphitization was performed by computing the degree of graphitization of the individual ingredients and the processed C/C composite at different stages. The degree of graphitization of the C/C composite system is the key parameter. It is the real measure of the extent to which the C/C composite system has transitioned from turbostratic to graphitic structure. Additionally, it determines the properties of the particular C/C composite system. A higher degree of graphitization results in higher thermal and electrical properties, slightly lower mechanical properties and improved tribological properties [36].

The degree of graphitization of all the ingredients except P75 was found to be either –ve or very low. This suggests the amorphous nature of the ingredients. Further, the degree of graphitization of the C/C composite without the graphitization step was found to be in the medium range. However, the heat treatment of the C/C composite samples at 3000°C resulted in more than a 70% degree of graphitization.

Above 43%, the degree of graphitization of a C/C composite system typically shows symmetrical peaks [36]. However, this generalization is not appropriate for our case because it was derived for a system where the carbon matrix was obtained from a single graphitizable source, whereas we derived the carbon matrix from two distinct phases, one which produces GC and the other NGC. Therefore, in spite of exhibiting a degree of graphitization above 70%, the XRD pattern may contain asymmetrical peaks due to the presence of a good amount of NGC (approximately 30%). And these asymmetrical peaks may also contain several components, among which there may be large differences in the extent of graphitization.

3.2. Thermal properties

Thermal properties are the most structurally dependent properties, and are influenced by both the macrostructure and the microstructure of the material. Since a C/C composite is a two phase material system, their macrostructure and microstructure can vary a lot, and hence their thermal properties as well [23]. The processing routes used to manufacture C/C can result in different matrix characteristics in terms of porosity network, micro-structural organization and heterogeneity, which can all influence their thermal properties [39]. Further, these properties are greatly dependent on the types of reinforcement and matrix. The important thermal properties which determine the performance of a material are thermal conductivity, thermal diffusivity, specific heat and the CTE. Having accurate and directional measurements of these properties is very important to its eventual application. Knowledge of these properties becomes critically essential when systems like randomly oriented fiber reinforced composites with hybrid reinforcement and hybrid matrix are being considered for potential applications.

3.2.1. Specific heat

It is known that the types of ingredients present in a system can influence its specific heat (C_p) [23]. In the present composite system the ingredients are different in many aspects. Therefore, to check the uniformity of the hybrid carbon fibers and hybrid matrixes in the composite system, measurements to determine the specific heat of specimens with varying thickness were carried out. Since the specific heat is independent of the shape, size and geometry of the specimen, variations due to different thicknesses will indicate that the constituents in the composite system are distributed non-uniformly.

We started by measuring the specific heat of the specimens from 50 to 600°C with various thicknesses from 2 to 5 mm. The specific heat measured as a function of varying thickness is shown in Fig. 6. From Fig. 6, it can be observed that there is only a marginal difference in the specific heat of the samples throughout the test temperature range. This indicates that the process employed for the fabrication of the C/C composite facilitated the uniform distribution of the ingredients used for fabrication.

From Fig. 7, it can be observed that the specific heat of the samples varies with the processing stages. The specific heat of the samples just after the primary HP method step is higher than that after the secondary ITC method step. The shows that the type of carbon matrix greatly influences the thermal absorbance property. This might have happened because there was more GC

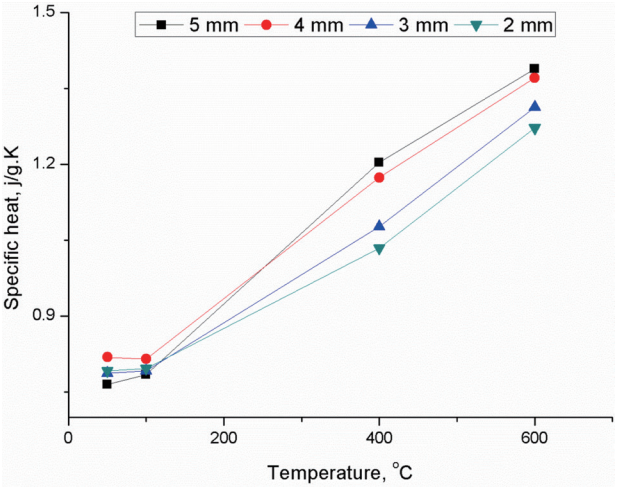

Fig. 6. Variation in specific heat with test temperature for different thicknesses.

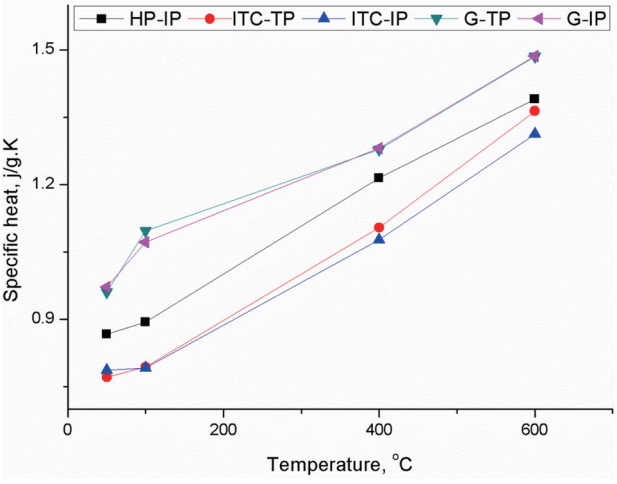

Fig. 7. Variation in specific heat with test temperature for different processing stages and directions. HP, hot-pressing; IP, in-plane; ITC, impregnation thermosetting carbonization; TP, through-plane; G, graphitization.

present in the sample after the primary HP method step as compared to the secondary ITC method. A glassy matrix was formed during the secondary method whereas a graphitic matrix was formed during the primary HP method. The highly ordered graphitic fibers and matrix have a higher thermal absorbance than non-graphitic fibers and matrix [23]. This difference can be seen in Fig. 7. The specific heat of the samples further increased after graphitization.

Further, the thickness direction doesn't affect the thermal absorbance property. In the literature [23] it was reported that the usage of short fibers does affect the thermal absorbance property. The main reason given for this was the disturbance created in the matrix structure by the short fibers. However, this sort of disturbance in the thermal absorbance property was not observed in our case. The probable reason may be the aspect ratio. The length of milled fiber used in the literature [23] was around 0.5 mm whereas we didn't use a fiber lower than 3 mm. Therefore, the reinforcement we used might have avoided creating a disturbance w.r.t. thermal absorbance. Further, the specific heat of the samples after graphitization was found to be well in accordance with the literature.

3.2.2. Thermal diffusivity

The thermal conductivity of the system chiefly depends upon density, specific heat and thermal diffusivity. The density and specific heat, as discussed in previous sections, were found to be independent of direction and thickness. Therefore, if any change in thermal conductivity is observed for such samples it may be because of a variation in thermal diffusivity.

Thermal diffusivity is representative of how well a material achieves uniform temperature [26]. As discussed in previous sections, density and specific heat were found to vary with processing cycles and the ingredients used. Therefore, the variation in conductivity as a function of processing cycle and ingredients can be significant. For this reason, it is important to have a good understanding of thermal diffusivity in order to understand the conduction mechanism of heat in the C/C composite system.

Heat conduction in a C/C composite is governed by the vibration of the crystal lattice, as per quantum theory. The lattice vibration is best described by phonon interactions. These phonons occur in two types, optic and elastic. The optic phonon is test temperature dependent and significant when the test temperature is very high. Since our test temperature was low (600°C), its contribution to energy transmission is small and can be ignored. Consequently, the energy transmission in the composite depends on acoustic phonons or elastic phonons [26].

The phonon interactions in a C/C composite can be divided into 3 categories: 1, phonon-phonon interactions; 2, phonon-defect interactions; 3, phonon interface interactions. The trend in thermal diffusivity as a function of test temperature for densified samples of varying thickness is shown in Fig. 8. From Fig. 8, it can be seen that the thermal diffusivity of all the samples increased as the test temperature was increased from 50 to 100°C, and then it decreased continuously with test temperature, reaching the lowest value at 600°C. This trend in thermal diffusivity can be attributed to the increase in phonon vibration frequency due to the increase in temperature. The higher vibration frequency caused more rapid collisions and as a consequence the mean free path decreased. This resulted in the drop in thermal diffusivity at higher temperature [26]. A similar trend was noticed irrespective of test specimen thickness. However, the diffusivity was found to decrease marginally with the thickness of the C/C specimens.

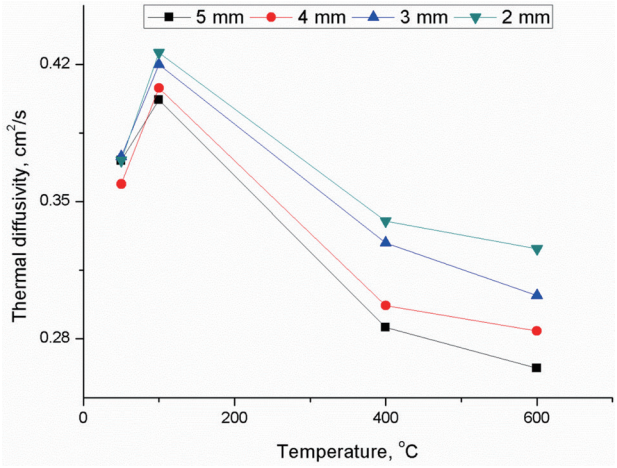

Fig. 8. Variation in thermal diffusivity with test temperature for different thicknesses.

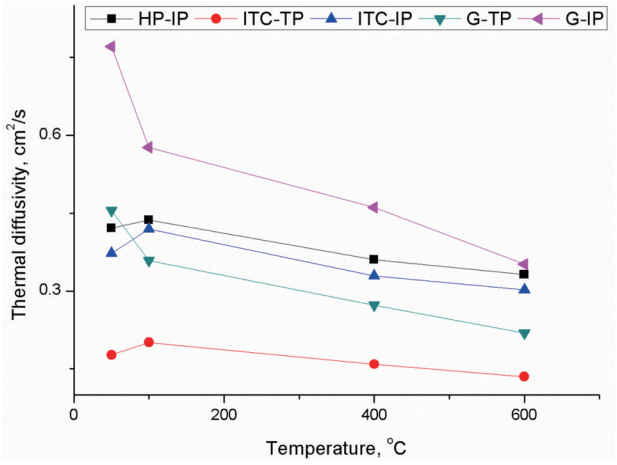

Fig. 9. Variation in thermal diffusivity with test temperature for different processing stages and directions. HP, hot-pressing; IP, in-plane; ITC, impregnation thermosetting carbonization; TP, through-plane; G, graphitization.

The trend in the thermal diffusivity of the samples processed under different conditions, in both the through-plane and the in-plane directions as a function of temperature, is shown in Fig. 9. The samples after the HP and ITC method steps, irrespective of their direction, showed a similar trend, like the samples with different thicknesses discussed in the previous section. However, the variation in the thermal diffusivity can be seen as a function of processing conditions and the directions.

The interesting thing is that, like specific heat, the thermal diffusivity of the samples after the HP method step was found to be greater than it was after the low-pressure ITC method step. This can be attributed to the presence of more graphitic carbon in the samples after the primary method compared to the secondary method.

The trend exhibited by the samples after graphitization was also different than that shown after the primary and secondary methods. In the graphitized samples, the thermal diffusivity was found to decrease with temperature. Similar observations have been reported in the literature [26]. The large difference in the thermal diffusivity of the samples in the in-plane and through-plane directions can be attributed to the presence of a large number of continuous channels for phonon transmission in the in-plane direction, as a result of the alignment of most of the carbon fibers in the x-y direction due to the higher aspect ratio and unidirectional load [26].

3.2.3. Thermal conductivity

Detailed insights about the thermal conductivity of this new system were explored by first studying its dependency on the thickness of the test specimens. As mentioned above, the main objective in studying the thermal conductivity as function of thickness was to verify the uniform distribution of ingredients in the hybrid/hybrid composite system. Fig.10 shows the thermal conductivity in the in-plane direction as a function of temperature for densified samples having different thicknesses. It can be clearly seen from Fig.10 that irrespective of their thickness, the trends shown by the samples are almost the same. This suggests that the material made here had a uniform distribution of ingredients.

The thermal conductivity as a function of the test temperature of samples after the HP method, ITC method and graphitization steps, both parallel (x) and perpendicular (z) to the fiber array, is shown in Fig. 11. The graphitized samples have higher conductivity up to a test temperature of 100°C. The in-plane thermal conductivity of the graphitized samples remains high over the entire test temperature range, whereas through-plane conductivity falls on or after a test temperature of 400°C, as compared to those after the ITC method step.

The main reason behind the higher conductivity of the samples after graphitization as compared to that after ITC can be attributed to the microstructure of the matrix. The graphitization operation makes the microstructure of the matrix smoother [40] and increases the crystallite size. As a consequence, the phonon mean free path is dominated by phonon-phonon interactions [26]. Therefore, the thermal diffusivity and thermal conductivity at a given temperature is higher for the samples after graphitization than after the ITC method. The huge difference between the in-plane and through-plane conductivity of the samples, irrespective of their processing conditions, can be attributed to the availability of a smaller number of continuous heat conduction channels in the through-plane direction. This is because most of the carbon fibers are aligned in the in-plane direction [26], and the microstructure is more disturbed in the through-plane direction as compared to the in-plane direction [24].

Interestingly, the thermal conductivity of the samples showed an increasing trend as a function of temperature as compared to those after graphitization. All the samples after the HP method and ITC method steps, irrespective of test direction, showed a similar trend. From Fig. 11, it can be seen that initially, conductivity increases steeply as the test temperature increases from 50 to 100°C. Thereafter, the net increase in thermal conductivity remains, but the rate of increase falls comparatively. This particular trend showing an increase in thermal conductivity with

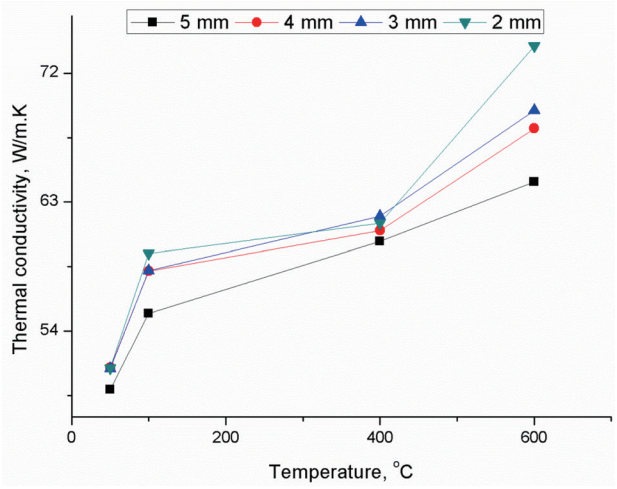

Fig. 10. Variation in thermal conductivity with test temperature for different thicknesses.

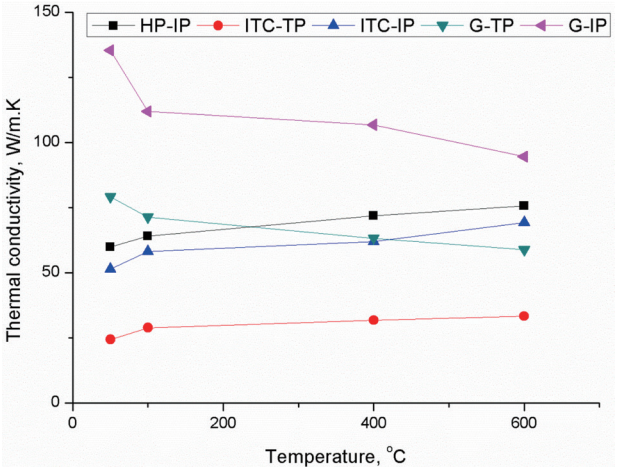

Fig. 11. Variation in thermal conductivity with test temperature for different processing stages and directions. HP, hot-pressing; IP, in-plane; ITC, impregnation thermosetting carbonization; TP, through-plane; G, graphitization.

test temperature is different than that reported for CVI-densified composites [41].

In fibrous materials comprised of amorphous carbon, heat transfer by solid conduction, radiation and by gases present in the pores contribute to the overall thermal conductivity. Further, as reported in the literature [41], the dominance of radiation conduction increases as the test temperature increases, and as a result, an increase in thermal conductivity takes place. Further, the crystallite size of amorphous carbon is small, and in the samples after the HP and ITC method steps, most of the carbon is amorphous. Therefore, the phonon mean free path is determined by phonon-defect interactions, resulting in a thermal conductivity which is low compared to the graphitized samples, and which increases with test temperature [41].

3.2.4. Coefficient of thermal expansion

The CTE for both the in-plane and through-plane directions

Table 2. CTE variation with temperature ranges

Temperature range	CTE ($\times 10^{-6}$)	
	Through-plane	In-plane
RT-350	6.08	-
RT-600	5.05	-
RT-800	4.63	-
RT-900	4.01	-
RT-1000	3.50	0.9

CTE, coefficient of thermal expansion

after the ITC method step is shown in Table 2. It can be seen that the in-plane direction CTE is very low in the range from RT-1000°C. This is because most of the fibers are aligned in the in-plane direction. As a consequence, the net CTE of the composite in the in-plane direction is governed by the axial expansion of the fibers, and axial expansion of the fibers is generally very low or negative. The CTE in the through-plane direction is comparatively high in the same temperature range. Further, the CTE decreases as the temperature increases. This can be attributed to the –ve expansion shown by the graphitic part of the constituents at higher temperature.

3.3. Electrical properties

Over the last few decades, the mechanical and thermal properties of C/C composites have been widely investigated. Their excellent combination of thermal and mechanical properties make the C/C composites suitable candidates for the thermo-structural applications for which they were initially developed. Further, their good electrical conductivity combined with light weight makes them potential alternatives to metals in several applications such as satellite and PEM fuel cell components. However, until now, a detailed study of their electrical performance has not been done. More specifically, measurements of the electrical properties of short carbon fiber reinforced C/C composites are not available. Clearly, knowledge of their electrical properties is a significant factor in deciding their utility for application as the bipolar plate of a PEM fuel cell or components of satellites. Therefore, a thorough investigation of the electrical conductivity of the new system was carried out.

The electrical conductivity in the x-y-plane and z-plane was measured as a function of heat treatment temperatures, and the results are shown in Table 3. The vast difference between the in-plane and through-plane conductivities of the composite after the low-pressure ITC method step can be seen. The main reason behind this difference is the availability of more conduction paths in the x-y plane due to the alignment of carbon fibers in the plane as a result of uni-direction pressing during the HP method step, and the higher aspect ratio of carbon fibers. The majority of the reinforcement is graphitic and the alignment of the graphite basal planes in the carbon fiber takes place along the fiber axis. This is the main cause of the higher conductivity exhibited by carbon fibers in the fiber axis direction, as compared to the transverse direction. Their alignment in the x-y plane in the

Table 3. Variation in electrical conductivity for both in-plane and through-plane directions with processing stages

Processing stages	Electrical conductivity (S/cm^2)	
	Through-plane	In-plane
ITC method	190	595
Graphitization	565	1180

ITC, impregnation thermosetting carbonization

composite system imparts higher conductivity to the composite system in the x-y plane. Further, the carbon matrix adjacent to the carbon fiber filaments might also have aligned along the filament axis, which would also contribute to the higher x-y plane conductivity.

As is evident from Table 3, after graphitization at elevated temperature, the electrical conductivity in both directions has increased by a factor of 2. This can be attributed to the fact that the majority of the matrix (PCM, 70.31%) which was graphitizable before graphitization, becomes graphitic after graphitization. As a consequence, conduction was also facilitated by the carbon matrix. After graphitization, the system became like a network of conducting inclusions lying in a conducting matrix. This subsequently facilitated conduction as per the percolation theory, where conductive paths are in physical contact with each other.

In this case, after graphitization, the PCM acted as a conducting path along with P75 carbon fibers, resulting in a 2 fold increase in the conductivity [42].

However, before graphitization the system has a lower percentage of graphitic reinforcement (31.97%, P75) along with glassy reinforcement (12.92%, T800) in the mixture of GC matrix (38.75%, PCM) and glassy carbon matrix (16.36%, SCM). This condition facilitates conduction by quantum tunneling. The presence of the glassy reinforcement, glassy matrix and graphitizable matrix would have created contact resistance within the conductive path between two carbon fiber filaments [42].

4. Conclusions

A detailed characterization of the thermo-electrical properties and physical properties of short fiber carbon/carbon (C/C) composite was carried out. Though the dispersion and random distribution of carbon fibers in the carbon matrix was excellent, the alignment of carbon fibers resulting from unidirectional pressing dominated the thermo-electrical properties. The dominance of alignment remained even after graphitization, which produced a 2 fold increase in performance (electrical conductivity, from 190 to 565 and from 595 to 1180, for the through-plane and in-plane directions, respectively). The CTE was found to decrease with increasing temperature. Interestingly, thermal conductivity as a function of test temperature was found to increase with temperature after the HP and ITC method steps, and decreased after graphitization. Further, the graphitization resulted in excellent carbon purity and a moderate increase in density.

Conflict of Interest

No potential conflict of interest relevant to this article was reported.

Acknowledgements

The authors are thankful to the testing divisions of Vikram Sarabhai Space Centre for their timely support in the characterization of the C/C composite compacts. The Authors are grateful to Mr. Mukesh Bhai, Mr. Hentry, Mr. V. K. Vineeth, Mr. Omendra Mishra, Mr. S. Babu, Mr. C. Simon Wesley, Mr. V. Chandrasekaran, Dr. P. P. Sinha, Dr. Koshy M. George, Mr. K.S. Abhilash, Mr. Vijendra Kumar, Mr. Biswa Ranjan Mohanty, Ms. Bismi Basheer, Ms. Soumyamol, Ms. Dhanya, Mr. Ranjith, Mr. Sushant K. Manwatkar, Dr. S.V.S. Narayna Murthy and Dr. P. Ramesnarayan for their valuable suggestions, assistance and support in bringing out this piece of work.

References

[1] Xiong X, Huang BY, Li JH, Xu HJ. Friction behaviors of carbon/carbon composites with different pyrolytic carbon textures. Carbon, **44**, 463 (2006). https://doi.org/10.1016/j.carbon.2005.08.022.

[2] Fitzer E. The future of carbon-carbon composites. Carbon, **25**, 163 (1987). https://doi.org/10.1016/0008-6223(87)90116-3.

[3] Buckley JD. Carbon/carbon: an overview. Ceram Bull, **67**, 364 (1998).

[4] Wang Q, Han XH, Sommers A, Park Y, Joen CT, Jacobi A. A review on application of carbonaceous materials and carbon matrix composites for heat exchangers and heat sinks. Int J Refrig, **35**, 7, (2012). https://doi.org/10.1016/j.ijrefrig.2011.09.001.

[5] Gandikota V, Jones GF, Fleischer AS. Thermal performance of a carbon fiber composite material heat sink in an FC-72 thermosyphon. Exp Therm Fluid Sci, **34**, 554 (2010). https://doi.org/10.1016/j.expthermflusci.2009.11.008.

[6] Raunija TSK, Babu S, Wesley CS. A process of producing carbon/carbon composite. Indian Patent, Application No. 1713/CHE/2012.

[7] Raunija TSK, Babu S. Randomly oriented carbon/carbon composite. AIP Conf Proc, **1538**, 168 (2013). https://doi.org/10.1063/1.4810050.

[8] Barabash V, Akiba M, Bonal JP, Federici G, Matera R, Nakamura K, Pacher HD, Rödig M, Vieider G, Wu CH. Carbon fiber composites application in ITER plasma facing components. J Nucl Mater, **258-263**, 149 (1998). https://doi.org/10.1016/s0022-3115(98)00267-0.

[9] Antunes RA, de Oliveira MCL, Ett G, Ett V. Carbon materials in composite bipolar plates for polymer electrolyte membrane fuel cells: a review of the main challenges to improve electrical performance. J Power Sources, **196**, 2945 (2011). https://doi.org/10.1016/j.jpowsour.2010.12.041.

[10] Planes E, Flandin L, Alberola N. Polymer composites bipolar plates for PEMFCs. Energy Procedia, **20**, 311 (2012). https://doi.org/10.1016/j.egypro.2012.03.031.

[11] Yuan XZ, Wang H, Zhang J, Wilkinson DP. Bipolar plates for PEM fuel cells: from materials to processing. J New Mater Electrochem Syst, **8**, 257 (2005).

[12] Maheshwari PH, Mathur RB, Dhami TL. Fabrication of high strength and a low weight composite bipolar plate for fuel cell applications. J Power Sources, **173**, 394 (2007). https://doi.org/10.1016/j.jpowsour.2007.04.049.

[13] Ozturk A, Moore RE. Tensile fatigue behaviour of tightly woven carbon/carbon composites. Composites, **23**, 39 (1992). https://doi.org/10.1016/0010-4361(92)90284-2.

[14] Li C, Crosky A. The effect of carbon fabric treatment on delamination of 2D-C/C composites. Compo Sci Technol, **66**, 2633 (2006). https://doi.org/10.1016/j.compscitech.2006.03.025.

[15] Lucchesi AJ, Hay JC, White KW. Characterization of wake-zone tractions in an oxidation-inhibited carbon/carbon composite. Compos Sci Technol, **49**, 315 (1993). https://doi.org/10.1016/0266-3538(93)90062-l.

[16] Ko TH, Kuo WS, Chang YH. Influence of carbon-fiber felts on the development of carbon-carbon composites. Compos Part A Appl Sci Manuf, **34**, 393 (2003). https://doi.org/10.1016/s1359-835x(03)00053-8.

[17] Tzeng SS, Lin WC. Mechanical behavior of two-dimensional carbon/carbon composites with interfacial carbon layers. Carbon, **37**, 2011 (1999). https://doi.org/10.1016/s0008-6223(99)00074-3.

[18] Appleyard SP, Rand B. The effect of fibre–matrix interactions on structure and property changes during the fabrication of unidirectional carbon/carbon composites. Carbon, **40**, 817 (2002). https://doi.org/10.1016/s0008-6223(01)00204-4.

[19] Rao MV, Mahajan P, Mittal RK. Effect of architecture on mechanical properties of carbon/carbon composites. Compos Struct, **83**, 131 (2008). https://doi.org/10.1016/j.compstruct.2007.04.003.

[20] Shin HK, Lee HB, Kim KS. Tribological properties of pitch-based 2-D carbon-carbon composites. Carbon, **39**, 959 (2001). https://doi.org/10.1016/s0008-6223(00)00158-5.

[21] Luo R, Huai X, Qu J, Ding H, Xu S. Effect of heat treatment on the tribological behavior of 2D carbon/carbon composites. Carbon, **41**, 2693 (2003). https://doi.org/10.1016/s0008-6223(03)00291-4.

[22] Klett JW, Burchell TD, Bailey JL. Method for rapid fabrication of fiber preforms and structural composite materials. US Patent 5,871,838 (1999).

[23] Manocha LM, Warrier A, Manocha S, Sathiyamoorthy D, Banerjee S. Thermophysical properties of densified pitch based carbon/carbon materials: I. unidirectional composites. Carbon, **44**, 480 (2006). https://doi.org/10.1016/j.carbon.2005.08.012.

[24] Manocha LM, Warrier A, Manocha S, Sathiyamoorthy D, Banerjee S. Thermophysical properties of densified pitch based carbon/carbon materials: II. bidirectional composites. Carbon, **44,** 488 (2006). https://doi.org/10.1016/j.carbon.2005.08.013.

[25] Park JK, Kang TJ. Thermal and ablative properties of low temperature carbon fiber–phenol formaldehyde resin composites. Carbon, **40**, 2125 (2002). https://doi.org/10.1016/s0008-6223(02)00063-5.

[26] Luo R, Liu T, Li J, Zhang H, Chen Z, Tian G. Thermophysical properties of carbon/carbon composites and physical mechanism of thermal expansion and thermal conductivity. Carbon, **42**, 2887 (2004). https://doi.org/10.1016/j.carbon.2004.06.024.

[27] Raunija TSK, Manwatkar SK, Sharma SC, Verma A. Morphological optimization of process parameters of randomly oriented carbon/carbon composite. Carbon Lett, **15**, 25 (2014). https://doi.org/10.5714/cl.2014.15.1.025.

[28] Raunija TSK, Gautam RK, Sharma SC, Verma A. Yield behavior of matrix precursor and interaction with reinforcement in randomly

oriented carbon/carbon composite. New Carbon Mater, accepted (2017).

[29] Raunija TSK, Sharma SC. Influence of hot-pressing pressure on the densification of short-carbon-fiber-reinforced, randomly orientedd carbon/carbon composite. Carbon Lett, **16**, 25 (2015). https://doi.org/10.5714/cl.2015.16.1.025.

[30] Raunija TSK, Gautam RK, Sharma SC, Verama A. Rapid fabrication of high density C/C composite by coupling of processess. Adv Mater Lett, **8**, 136 (2017). https://doi.org/10.5185/amlett.2017.6673.

[31] Raunija TSK. Influence of temperature and time shifts on the densification of randomly oriented carbon/carbon composite. Def Sci J, **65**, 411 (2015). https://doi.org/10.14429/dsj.65.8135.

[32] Raunija TSK, Sharma SC, Verama A. Yield enhancement of matrix precursor in short carbon fiber reinforced randomly oriented carbon/carbon composite. Carbon Lett, **19**, 57 (2016). https://doi.org/10.5714/cl.2016.19.057.

[33] Raunija TSK, Gautam RK, Bhradwaj VM, Nandikesan N, Shaneeth M, Sharma SC, Verama A. Low cost and rapidly processed randomly oriented carbon/carbon composite bipolar plate for PEM fuel cell. Fuel Cells, **16**, 801 (2016). https://doi.org/10.1002/fuce.201600079.

[34] Raunija TSK. A novel macine and method for milling continuous fibers. Indian J Eng and Mater Sci, **22**, 541 (2015).

[35] Lee YH, Bulletin of College of Engineering, National Taiwan University. Available from: http://www.eng.ntu.edu.tw/eng/chinese/bulletin/n89/n89-11.pdf.

[36] Zou L, Huang B, Huang Y, Huang Q, Wang C. An investigation of heterogeneity of the degree of graphitization in carbon-carbon composites. Mater Chem Phys, **82**, 654 (2003). https://doi.org/10.1016/s0254-0584(03)00332-8.

[37] Biscoe J, Warren BE. An X-ray study of carbon black. J Appl Phys, **13**, 364 (1942). https://doi.org/10.1063/1.1714879.

[38] Savage GM. Carbon-Carbon Composite. London, Chapman and Hall, 323 (1992).

[39] Fitzer E, Manocha LM. Carbon Reinforcements and Carbon/Carbon Composites, Berlin Springer, New York, 97 (1998).

[40] Dekeyrel A, Dourges MA, Weisbecker P, Pailler R, Allemand A, Ténèze N, Epherre JF. Characterization of carbon/carbon composites prepared by different processing routes including liquid pitch densification process. Compos Part A Appl Sci Manuf, **49**, 81 (2013). https://doi.org/10.1016/j.compositesa.2013.02.010.

[41] Baxter RI, Rawlings RD, Iwashita N, Sawada Y. Effect of chemical vapor infiltration on erosion and thermal properties of porous carbon/carbon composite thermal insulation. Carbon, **38**, 441 (2000). https://doi.org/10.1016/s0008-6223(99)00125-6.

[42] Ounaies Z, Park C, Wise KE, Siochi EJ, Harrison JS. Electrical properties of single wall carbon nanotube reinforced polyimide composites. Compos Sci Technol, **63**, 1637 (2003). https://doi.org/10.1016/S0266-3538(03)00067-8.